Low-Temperature Sublattice Magnetization of Antiferromagnetic $CrCl_3$†

ALBERT NARATH
Sandia Laboratory, Albuquerque, New Mexico
(Received 8 April 1963)

The temperature dependence and the magnetic-field dependence of the $CrCl_3$ sublattice magnetization have been studied in the temperature range 0.39–4.02°K by means of the Cr^{53} nuclear magnetic resonance. The experimental results are in quantitative agreement with predictions of the isotropic Heisenberg exchange model in the low-temperature spin-wave approximation. The antiferromagnetic interlayer-exchange interaction in this hexagonal layer-type crystal is shown to be sufficiently weak, compared to the ferromagnetic intralayer-exchange interaction, to justify its treatment as an effective anisotropy field. In addition to the exchange interactions, both dipolar and single-ion, $D(S^z)^2$, anisotropies are required to fit the data. The resulting two-dimensional ferromagnetic model accurately accounts for the strong temperature dependence of the sublattice magnetization and the approach of this dependence to linearity with increasing temperature. A fit of the theory to the experimental data gives an intralayer exchange constant $J/k=4.52\pm0.05$°K. The intensity enhancement of the Cr^{53} resonance in weak external magnetic fields, as well as in zero field, is discussed. The strong field-induced enhancement is explained by a domain rotation model which is based on the torque exerted by the driving field H_1 on the net field-induced magnetization, in the presence of a restoring force provided by a weak magnetocrystalline anisotropy ($K\sin^2 3\theta$) in the (001) plane. Comparison of calculated and observed intensities as a function of field strength yields $K=150\pm50$ ergs/cm³ and a spin flopping transition in the (001) plane at a field strength of ~160 Oe. The enhancement mechanism in external fields leads to selective excitation resulting in observable splittings of the nuclear resonance in polycrystalline samples when $H_1\|H$. The parallel magnetic susceptibility of the $CrCl_3$ spin system has been calculated from these splittings at several temperatures between 1 and 4°K. The results (e.g., 0.28 ± 0.01 emu/mole at 4.00°K) agree within experimental error with susceptibilities calculated from the spin-wave model using the interaction constants obtained from the temperature dependence of the sublattice magnetization.

I. INTRODUCTION

ZERO-FIELD nuclear magnetic resonance of magnetic ions in magnetically ordered systems provides a powerful tool for the study of the collective modes of excitation in such systems. The accuracy afforded by this method in determining the relative intrinsic magnetization near saturation makes it possible, in favorable cases, to correlate the experimental results with predictions of the Heisenberg exchange Hamiltonian[1] in the low-temperature spin-wave approximation.[2–4] The metamagnetic iron-group chlorides provide a particularly interesting application of this theory because of their rather unique magnetic properties.[5] These hexagonal layer-type compounds exhibit large field-dependent magnetic susceptibilities in the ordered state. This behavior is explained by weak antiferromagnetic exchange forces acting between hexagonal layers which are ordered ferromagnetically by relatively strong intralayer exchange interactions. The weak interlayer coupling results in a large net magnetization in the presence of magnetic fields of only moderate strength. These properties are most pronounced in $CrCl_3$. In an earlier report[4] it was proposed that the antiferromagnetic interlayer-exchange interaction in this compound is sufficiently weak to be included in an effective anisotropy field acting on each spin. The resulting two-dimensional ferromagnetic model predicts a strong, nearly linear temperature dependence of the sublattice magnetization. The observed temperature dependence of the Cr^{53} zero-field nuclear resonance frequency between 1.23 and 4.02°K was found to follow the predictions quite closely. In addition, the model predicts a sublattice magnetization with strong magnetic-field dependence arising from the well-known fact that a two-dimensional ferromagnetic system is unstable toward thermal excitations except in the presence of anisotropy or a magnetic field.[2]

The high sensitivity to external and internal perturbations which is thus predicted for the $CrCl_3$ spin system makes it an attractive system for study. An added attraction is the simple form which the spin Hamiltonian takes since the Cr^{3+} orbital moment is almost completely quenched ($g=2.00$) in the predominantly octahedral crystal field of $CrCl_3$. Furthermore, in the temperature range below 4°K lattice expansion effects should be negligible. One, therefore, expects the hyperfine coupling constant to be temperature-independent and, hence, expects the hyperfine field to give an accurate measure of the sublattice magnetization. In view of these considerations it seemed desirable to study the low-temperature magnetic behavior of $CrCl_3$ in more detail than we had done previously.

We have extended the Cr^{53} resonance studies to lower temperatures in order to check the validity of the two-

† Work performed under the auspices of the U. S. Atomic Energy Commission.

[1] W. Heisenberg, Z. Physik **49**, 619 (1928).
[2] J. Van Kranendonk and J. H. Van Vleck, Rev. Mod. Phys. **30**, 1 (1958).
[3] A. C. Gossard, V. Jaccarino, and J. P. Remeika, Phys. Rev. Letters **7**, 122 (1961).
[4] A. Narath, Phys. Rev. Letters **7**, 410 (1961).
[5] C. Starr, F. Bitter, and A. R. Kaufmann, Phys. Rev. **58**, 977 (1940); C. Starr, *ibid.* **58**, 984 (1940); J. Kanamori, Progr. Theoret. Phys. (Kyoto) **20**, 890 (1958); references to earlier work are contained in these papers.

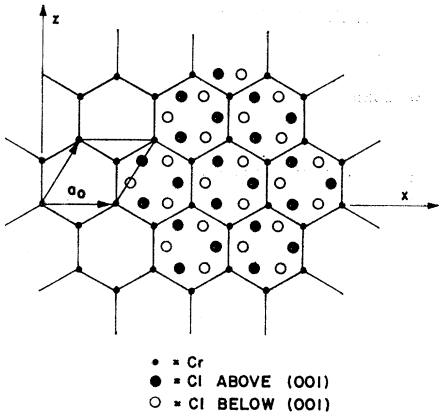

FIG. 1. Projection of $CrCl_3$ "sandwich" on (001) plane.

dimensional model at temperatures where the interlayer interaction might be expected to cause large deviations from the predictions of the simple model. Studies of the intensity enhancement of the Cr^{53} nuclear resonance in weak external magnetic fields have provided a measure of the anisotropy in the hexagonal basal plane and have made it possible to determine the parallel magnetic susceptibility of $CrCl_3$ in polycrystalline samples. We have compared our results with calculations for the following models: (1) two-dimensional ferromagnetic spin-wave model in the presence of an effective anisotropy field; (2) three-dimensional ferro-antiferromagnetic model in the presence of an effective anisotropy field; and (3) two-dimensional ferromagnetic model with explicit treatment of a uniaxial magneto-crystalline anisotropy and intralayer dipole-dipole interactions.

Anhydrous $CrCl_3$ has a hexagonal unit cell of space group D_3^5 containing six molecules.[6] The structure consists of a honeycomb array of chromium ions sandwiched between two close-packed layers of chlorine ions (Fig. 1). These sandwiches are stacked together in such a way as to produce an almost undistorted face-centered cubic packing of chlorine ions. $CrCl_3$ exhibits a λ-type specific-heat anomaly at 16.8°K[7] and a susceptibility maximum near 20°K. A very detailed single-crystal magnetic susceptibility investigation has recently been reported by Bizette, Terrier, and Adam[8] ($\chi_\perp = 5.5$ emu/mole below 4°K in zero field). The magnetic structure has been elucidated by Cable, Wilkinson, and Wollan[9] using neutron diffraction techniques. The moments were found to lie in the (001) planes with adjacent ferromagnetic layers being antiparallel.

[6] N. Wooster, Z. Krist. **74**, 363 (1930).
[7] W. N. Hansen and M. Griffel, J. Chem. Phys. **28**, 902 (1958).
[8] H. Bizette, C. Terrier, and A. Adam, Compt. Rend. **252**, 1571 (1961).
[9] J. W. Cable, M. K. Wilkinson, and E. O. Wollan, J. Phys. Chem. Solids **19**, 29 (1961).

II. EXPERIMENTAL PROCEDURES

All measurements reported here were carried out on polycrystalline samples. Because of the soft, fragile nature and the pronounced plate-like crystal habit of $CrCl_3$ we have been unable to obtain single crystals of sufficient size for our nuclear resonance studies. Most of the measurements utilized a dense polycrystalline sphere of ~7-mm diam which had the individual c axes oriented parallel throughout its volume.[10] Preliminary experiments were carried out on powdered samples. Because of the flaky character of $CrCl_3$ it was possible to achieve almost perfect preferred alignment of the c axes in these samples by carefully pressing the powders into flat-bottomed holders. In this way both rf and static fields could be applied in the (001) plane (i.e., in the plane of the moments). This field configuration was used in all of our experiments. The pressed specimens were prepared both from commercial $CrCl_3$ (containing up to 0.6% Fe) and samples made by vacuum sublimation of material obtained from the chlorination of chromium metal (99.99% purity.) These were used primarily to check the validity of the relatively large demagnetization corrections which were applied to the data from our field-dependence measurements. The pressed-flake data presented in this paper were obtained with sample geometries for which these corrections are presumed to be negligible.

The nuclear resonances were observed with a frequency swept FM marginal oscillator.[11] After synchronous detection the signals were displayed on a strip-chart recorder. Second-derivative presentations were used for frequency measurements and first derivative presentations were used to obtain integrated intensities. Weak fields were produced by a large solenoid calibrated against a Hall element. Measurements above 1 kOe utilized a 12-in. electromagnet. No attempt was made to cancel the earth's magnetic field in the zero-field experiments.

Temperatures between 1.0–4.0°K were attained with a standard nitrogen-jacketed helium Dewar. The pumping system consisted of a 47 cfm mechanical pump in series with a 310 cfm Roots blower (10:1 compression below 10 mm Hg). Below 1.0°K a recycling He^3 refrigerator was used. Its design was dictated by the need to change samples quickly and conveniently and by the requirement that the refrigerator not interfere with the operation of the tuned rf transmission system. A schematic of the refrigerator system is given in Fig. 2(a). A more detailed diagram of the condenser, evaporator, and sample chamber is shown in Fig. 2(b). The refrigerator consists of two main parts: (1) the He^3 system with compressor, condenser, evaporator, and associated supply lines, values and flanges; (2) the copper sample chamber which, sup-

[10] This sample was obtained from Clevite Corporation, Electronic Research Division, Cleveland, Ohio.
[11] R. G. Shulman, Phys. Rev. **121**, 125 (1960).

ported by the He^3 vapor-pressure thermometer bulb, is lowered through the 1-in.-i.d. He^3 exhaust line into the vacuum jacketed evaporator chamber. This arrangement permits samples to be removed without disturbing any of the soldered vacuum-tight joints of the He^3 system. The sample assembly is joined to the refrigerator by means of an "O"-ring seal at the top of the cryostat.

The He^3 compressor consists of a 2.3 liter/sec mechanical pump[12] and a small oil-diffusion pump coupled to a 2-in.-diam He^3 exhaust line. In order to guard against magnetic shielding in the field-dependence experiments, the lower portion of the inner and outer walls of the evaporator chamber (1.5-in. o.d., 1.0-in. i.d.) are constructed of copper. The $\frac{3}{16}$-in.-o.d. copper condenser is located inside the vacuum space and makes thermal contact with the He^4 bath through copper wires which pass through the outer wall of the jacket. The condenser valve and needle are made of stainless steel. The monel capillary (0.020 in. × 0.010 in. filled with 0.008-in. monel wire) passes the He^3 from the needle valve into the bottom of the evaporator. The vacuum jacket of the evaporator chamber is connected to the He^3 exhaust line through a valve, permitting the use of He^3 as exchange gas during cool-down to the He^4 bath temperature.

The outer shell of the sample chamber is sealed to the top of the sample assembly with low melting-point solder for easy removal. He^4 serves as exchange gas inside the chamber. Thermal contact with the bottom of the evaporator chamber is provided by a spring-loaded copper disk which slips over the protruding end of the capillary. Several copper wires pass between the disk and the sample chamber to assure isothermal conditions inside the evaporator. The He^3 thermometer tube carries several radiation baffles which also serve as supports for the balanced rf transmission line and the resistance thermometer leads. The rf leads near the sample chamber consist of 0.008-in. monel wire silver plated to a thickness of 0.0001 in.; copper wire is used in the upper portion of the cryostat.

Temperatures to slightly below 0.4°K are easily achieved and can be maintained for 5–7 h using a He^3 gas charge of ~1 liter STP and a He^4 bath capacity of 1.5 liters. Temperature measurements were based on the $He^3(T_E)$ and $He^4(T_{58})$ vapor pressure scales, using carbon and germanium resistance thermometers as secondary standards, and have an estimated accuracy of ±0.01°K throughout the experimental range.

III. SUBLATTICE MAGNETIZATION

The simplest model which can account for the observed temperature dependence of the $CrCl_3$ sublattice magnetization is a two-dimensional isotropically exchange-coupled lattice in the presence of an effective anisotropy field. The weak interlayer-exchange interaction is treated as part of the effective field. The Hamiltonian for such a system is given by

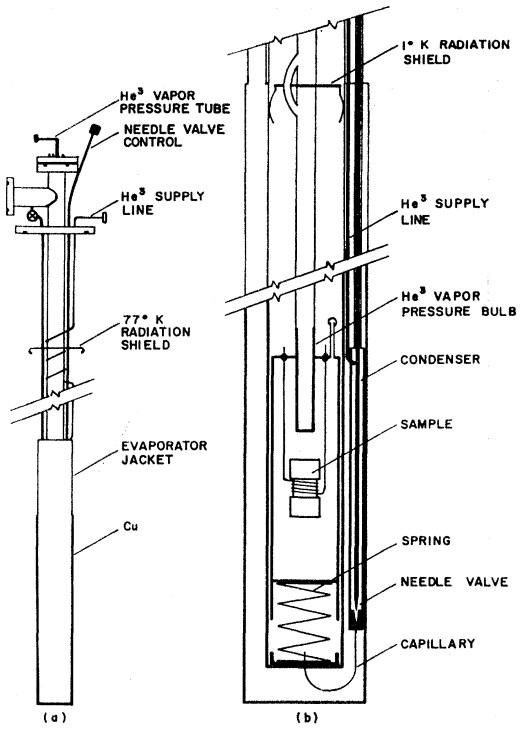

FIG. 2. Schematic of recycling He^3 cryostat.

$$\mathcal{H}_E=-\sum_{ii',pp'} J_{ii',pp'}\mathbf{S}_{ip}\cdot\mathbf{S}_{i'p'}-g\beta H_A\sum_{ip}S_{ip}{}^z, \quad (1)$$

where i numbers the cell and $p=1$, 2 designates the two inequivalent sites in the unit cell of the two-dimensional honeycomb lattice (Fig. 1). The anisotropy field is denoted by H_A. We shall consider only nearest neighbor exchange interactions. The first sum in (1) is, therefore, restricted to nearest neighbor Cr^{3+} pairs and J, the exchange-coupling coefficient, can be taken outside the sum. Furthermore, from the symmetry of the lattice it can be seen that $p\neq p'$. In the low-temperature spin-wave approximation of Holstein and Primakoff[13] the eigenvalues of (1) are

$$E(n_{\mathbf{k}s})=E_0+\sum_{\mathbf{k}s}\lambda_{\mathbf{k}s}n_{\mathbf{k}s};\quad n_{\mathbf{k}s}=0,\ 1,\ 2,\cdots$$
$$E_0=-2NS(g\beta H_A+3JS), \quad (2)$$

where $\mathbf{k}$ is the wave vector of the normal modes which fall into two branches designated by $s=1$, 2, and N is the number of cells in the system. $S=\frac{3}{2}$ is the effective spin angular momentum of the chromium ion. The spin-wave energies are

$$\lambda_{\mathbf{k}s}=g\beta H_A+2JS\{3+(-1)^s \times[\textstyle\sum_{mm'}\exp(-i\mathbf{k}\cdot(\mathbf{r}_m-\mathbf{r}_{m'}))]^{1/2}\}. \quad (3)$$

Here $\mathbf{r}_m$ denotes the vector from a given lattice point

[12] H. A. Reich and R. L. Garwin, Rev. Sci. Inst. **30**, 7 (1959).

[13] T. Holstein and H. Primakoff, Phys. Rev. **58**, 1098 (1940).

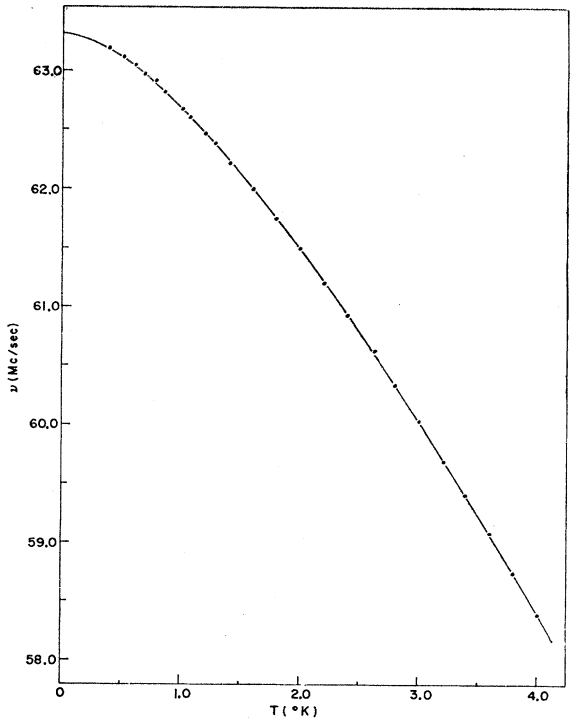

FIG. 3. Temperature dependence of the Cr^{53} NMR (central component of quadrupole triplet) in $CrCl_3$, in zero external field. Solid curve shows the best fit of the two-dimensional spin-wave model to the data.

to one of its three nearest neighbors. The sublattice magnetization is given by

$$M(T)=M(0)[1-(2NS)^{-1} \times\textstyle\sum_{ks}(\exp(\lambda_{ks}/kT)-1)^{-1}]. \quad (4)$$

In Ref. 4 we expanded (4) to order k^2 (long-wave limit) and obtained

$$M(T)=M(0)[1-\sqrt{3}kT(8\pi JS^2)^{-1} \times\sum_{n=1}^{\infty} n^{-1}\exp(-ng\beta H_A/kT)]. \quad (5)$$

A fit of the data to the approximate form (5) between 1.23–4.02°K gave $J/k=3.95$°K and $H_A=2700$ Oe. Subsequent calculations showed that the long-wave approximation introduced errors in ΔM of the order of 4.0% near 4.0°K; these deviations are larger than our experimental uncertainty of $\pm 0.2\%$ at this temperature. Also, since the anisotropy-induced deviation of ΔM from a linear temperature dependence is small above 1.23°K the fit is not too sensitive. We have, therefore, measured the zero-field Cr^{53} nuclear resonance on a new sample (dense polycrystalline sphere) between 0.39–4.02°K. In order to avoid errors in the comparison of experiment with theory, we have carried out exact numerical calculations using (3) and (4) rather than the approximate expression (5). We have assumed that the frequencies $\nu(T)$ are directly proportional to $M(T)$ in the temperature range studied. Zone-boundary effects and contributions to ΔM from the upper spin-wave branch were found to be negligible below 4°K. The sum over spin-wave states in (4) was replaced by a double integration within a circular zone of area equal to the real Brillouin zone. Only states belonging to the lower branch ($s=1$) were included. The integration was carried out over one quadrant of the zone for a 100×100 mesh using Simpson's rule. Convergence was assured by performing a series of trial calculations with different mesh sizes. The fit of the theory to the data was accomplished by trial and error using a least-squares criterion. A best fit is obtained for

$$\begin{aligned} J/k&=4.45\pm0.05\text{°K},\\ H_A&=2000\mp50\text{ Oe},\\ \nu(0)&=63.313\text{ Mc/sec}, \end{aligned} \quad (6)$$

with an rms deviation of ±0.012 Mc/sec largely due to scatter in our temperature measurements. The estimated uncertainties of J and H_A are not independent; the upper or lower signs are to be taken together. A plot of the results is given in Fig. 3. The measured frequencies were found to be independent of rf power level. Our value of J can be compared with that calculated from the molecular field model,

$$J=3kT_N/2zS(S+1), \quad (7)$$

where $T_N=16.8$°K is the Néel temperature of $CrCl_3$ and $z=3$ is the number of nearest neighbors in the (001) plane. From (7) we obtain $J/k=2.24$°K. The deviation of the spin-wave calculation from the molecular field result is in the expected direction but is unusually large.

We next examine the effect of the interlayer exchange on our low-temperature results. The magnitude of the interlayer-exchange constant (J_L) can be extimated from the measured perpendicular magnetic susceptibility by means of the molecular field approximation. The result is

$$J_Lz_L/k=-0.0649\text{°K}, \quad (8)$$

which is much smaller than the intralayer interaction ($Jz/k=13.3$°K). The interlayer exchange is equivalent to an exchange field

$$H_{ex}=2J_LSz_L/g\beta=1450\text{ Oe}, \quad (9)$$

which is smaller than H_A obtained in (6). We shall now treat the interlayer interaction explicitly using the following simplified lattice model. Each Cr^{3+} ion is assumed to be antiferromagnetically coupled to two neighbors, one directly above it and the other below it. This scheme is, of course, only an approximation to the actual stacking of the layers in $CrCl_3$. However, the small magnitude of the interaction justifies this simplification. We add to (1)

$$\mathcal{H}_L=-J_L\textstyle\sum_{jj',p}\mathbf{S}_{jp}\cdot\mathbf{S}_{j'p}. \quad (10)$$

The eigenvalues of the total Hamiltonian, $\mathcal{H}_E+\mathcal{H}_L$, to terms linear in the spin deviations, are easily obtained by the method of Wallace.[14]

$$E(n_{\mathbf{k}t})=E_0+\sum_{\mathbf{k}t}\omega_{\mathbf{k}t}(n_{\mathbf{k}t}+\tfrac{1}{2});\quad n_{\mathbf{k}t}=0,1,2,\cdots \quad (11)$$
$$E_0=-4N[g\beta H_A(S+\tfrac{1}{2})+S(S+1)(3J-2J_L)].$$

There are four branches, labeled by t, which divide into two degenerate pairs ($t=1$, 3 and $t=2$, 4) because of the assumed absence of an external field. The spin-wave energies are

$$\omega_{\mathbf{k}t}=[(A+(-1)^tB_{\mathbf{k}})^2-C_{\mathbf{k}}^2]^{1/2}, \quad (12)$$

with

$$A=g\beta H_A+6JS-4J_LS,$$
$$B_{\mathbf{k}}=2JS[\textstyle\sum_{mm'}\exp(-i\mathbf{k}_T\cdot(\mathbf{r}_m-\mathbf{r}_{m'}))]^{1/2},$$
$$C_{\mathbf{k}}=2J_LS\textstyle\sum_n\cos\mathbf{k}_L\cdot\mathbf{r}_n.$$

Here $\mathbf{k}_T$ is taken as the wave vector in the basal plane of the reciprocal lattice; $\mathbf{k}_L$ is normal to that plane. We have also defined $\mathbf{r}_n$ as the vector which connects nearest neighbors along the c axis. Using the transformation matrices obtained in the diagonalization of $\mathcal{H}$ we obtain for the sublattice magnetization

$$M(T)=M_s\left[1+\frac{1}{2S}-\frac{\eta}{NS}\right],$$
$$\eta=\tfrac{1}{4}\sum_{\mathbf{k}t}\left\{(\langle n_{\mathbf{k}t}\rangle+\tfrac{1}{2})\left[\frac{A+(-1)^tB_{\mathbf{k}}}{\omega_{\mathbf{k}t}}\right]\right\}, \quad (13)$$

where M_s is the saturation magnetization, and the average occupation numbers of the spin-wave modes are

$$\langle n_{\mathbf{k}t}\rangle=[\exp(\omega_{\mathbf{k}t}/kT)-1]^{-1}. \quad (14)$$

It can be seen that (13) reduces to (4) when $\omega_{\mathbf{k}t}$ approaches $\lambda_{\mathbf{k}s}$. We have analyzed our data according to (13) using the value for J_L obtained from the molecular-field theory (8). The numerical calculations were performed in the same manner as for the two-dimensional model. For the integration over $\mathbf{k}_L$ only 6 values between 0 and $3\pi/2c_0$ were required to give the desired accuracy, since excitations along that direction add little to the total energy. Applying this calculation to our data gives

$$J/k=4.50\pm0.05\,^\circ\mathrm{K},$$
$$H_A=750\mp50\ \mathrm{Oe}. \quad (15)$$

The calculated reduction of M(0) from its saturation value is only 0.01%. The value of J has remained essentially unchanged. It is evident, therefore, that the weak interlayer-exchange interaction has almost the same effect on the magnetization as an equivalent anisotropy field. A comparison of (6) and (15) leads to the conclusion that the interlayer interaction corresponds to an effective field of 1250 Oe, which is very close to the molecular field of Eq. (9). Although the interlayer-exchange interaction accounts for most of the total effective anisotropy of the two-dimensional model it is clear from (15) that an additional interaction is required to fit the observed temperature dependence of the sublattice magnetization. Before we attempt to account for this interaction, however, we should point out that the effective field approximation introduces rather serious errors into the energies of spin-wave modes with very small $\mathbf{k}$. In Sec. IV, we show that the in-plane anisotropy field is only of the order of 9 Oe. Hence, the frequency of the in-plane antiferromagnetic mode is nearly zero for $\mathbf{k}=0$, particularly since the interlayer-exchange coupling is very weak. The two-dimensional model, on the other hand, gives a gap, $g\beta H_A$, at $\mathbf{k}=0$. From (12) it can be seen that neglecting the $\mathbf{k}_L$ dependence of the spin-wave energies in our case becomes a good approximation only when the intralayer contribution to the energy becomes larger than that of the interlayer interaction; i.e., when

$$\Delta_{\mathbf{k}}>4J_LS, \quad (16)$$

where $\Delta_{\mathbf{k}}=6JS-B_{\mathbf{k}}$. Although the number of modes affected by the effective field approximation is quite small, their influence on the thermodynamic properties of our system is not entirely negligible even at temperatures much greater than $4J_LS/k$. This is due to the two-dimensional character of the spin-wave modes in $CrCl_3$ which makes the long-wave modes relatively more abundant than is the case for an isotropic three-dimensional system. This property of the $CrCl_3$ spin system not only accounts for the almost linear temperature dependence of the sublattice magnetization but also results in an unusually rapid decrease of $M(T)$ with increasing temperature (e.g., at $T/T_N=0.236$, $\Delta M=7.76\%$ in $CrCl_3$ whereas in[15] MnF_2 the corresponding value is only 1.22%). The same consideration leads to the prediction of a large parallel magnetic susceptibility since the relative contribution of an external magnetic field to the energy is largest for the long-wave modes. This point will be discussed further in Sec. V. Recently, Yoshimori[16] derived expressions for the frequencies of the normal modes appropriate to the metamagnetic iron-group chlorides by explicit treatment of the intralayer and interlayer-exchange interactions in the presence of a uniaxial anisotropy, $D(S^y)^2$. His model treats each ferromagnetic layer as a continuum and considers the discreteness of the lattice only along the c axis. The modes which result from this model correspond to those given by (11) for $t=1$, 3 although the former correctly take into account the out-of-plane anisotropy which removes the degeneracy of the two modes. This splitting, however, is very small in $CrCl_3$ because the magnitude of the anisotropy is very small. This is apparent from the small value of H_A in (15) and also from the small observed difference between the fields required for magnetic saturation perpendicular

[14] D. C. Wallace, Phys. Rev. **128**, 1614 (1962).

[15] V. Jaccarino and R. G. Shulman, Phys. Rev. **107**, 1196 (1957).

[16] A. Yoshimori, Phys. Rev. **130**, 1312 (1963).

and parallel to the c axis.[8] This difference is of the order of 2 kOe (or less if we correct the saturation field along the c axis of the single-crystal platelet for demagnetization). In fact, Dillon has concluded from his high-field ferromagnetic resonance measurements[17] that all of the anisotropy in $CrCl_3$ is due to shape effects. Unfortunately, Yoshimori's model treats the intralayer interaction only to order k_T^2. The error which is introduced by this approximation (for $CrCl_3$) falls, as we have shown, far outside our experimental uncertainty above 1°K. Fortunately, the interlayer interaction is extremely small; and therefore, for simplicity, we choose to retain the two-dimensional model for all of $\mathbf{k}$ space. However, we approximate the three-dimensional character of the extreme long-wave modes in the following way. We take the contribution of the interlayer-exchange interaction to H_A to be of the form

$$H_{ex}'(\mathbf{k})=\tfrac{1}{2}[\Delta_k(\Delta_k+g\beta H_{ex})^{-1}+1]H_{ex}, \qquad (17)$$

where H_{ex} is given by (9). We have tested this empirical form for the interlayer exchange interaction in the two-dimensional model (4) and compared the calculated values of $M(T)$ with those computed from the three-dimensional model (13). The agreement between the models is essentially within our experimental error even when H_A in (13) is taken equal to zero. For the latter case, the agreement is very poor if the effective field in the two-dimensional model is taken as H_{ex} rather than $H_{ex}'(\mathbf{k})$.

With the above approximation for the interlayer exchange interaction we now return to the question of the weak effective anisotropy implied by (15). A large contribution to it comes from the magnetic dipole-dipole interaction between Cr^{3+} spins. We have calculated the static dipole field at the Cr^{3+} position by direct summation on a CDC-1604 computer. Remainders were estimated by an integral approximation for the sums. We assumed a point dipole-moment corresponding to $3\mu_B$ localized on each chromium ion, and lattice constants of $a_0=5.952A$, $c_0=17.47A$.[9] The intralayer dipole sum H_D gives a field of 2254 Oe [isotropic in the (001) plane], while the contribution from the two adjacent layers is only $\sim$20 Oe. The latter value is too small to account for the observed interlayer coupling as had been suggested earlier.[4] These calculations ignore the effect of partial delocalization of the chromium spins due to covalent bonding. Since a large contribution to the interlayer sum comes from the three nearest neighbor chromium spins and since the nearest neighbor chlorine ions have octahedral symmetry with respect to the central Cr^{3+} ion, we expect a somewhat smaller interaction than calculated above. Despite this uncertainty, it seemed desirable to carry out an explicit treatment of the dipolar interaction in the point dipole approximation. In this calculation we have only considered intralayer contributions to the magnetic-dipole interactions. A quantum-mechanical treatment of ferromagnetic exchange in the presence of dipolar coupling has been given for primitive lattices by Holstein and Primakoff.[13] In Appendix I we derive the eigenvalues of the problem appropriate to our two-dimensional ferromagnetic honeycomb lattice. We take $H_A=H+H_{ex}'(\mathbf{k})$, where H is the external field. Because of the symmetry of the lattice the dipolar interaction gives no contribution to the spin-wave energy when $H_A=0$, $\mathbf{k}=0$. For finite $\mathbf{k}$, however, it gives a positive contribution. The numerical calculations of the magnetization [Eq. (49)] were carried out as follows. The $\mathbf{k}$-dependent dipole sums were computed separately as a function of $\mathbf{k}$ and stored on magnetic tape. One quadrant of a circular zone was used as before. Each $\mathbf{k}$ coordinate was divided into 100 intervals. The dipole sums were restricted to 1681 lattice points within a circular area, resulting in a maximum error (for small $\mathbf{k}$) of $\sim$1%. The dipole sums were used to calculate the eigenvalues which were required in the subsequent Simpson's rule integration to yield the relative sublattice magnetization. Inclusion of the upper spin-wave branch was again found to be unnecessary. Since the most time-consuming step (i.e., the computation of the dipole sums) was carried out only once, it was easy to repeat the calculation for different values of the parameters T and J. The results of the above numerical computations clearly show that the predicted low-temperature curvature of $M(T)$ greatly exceeds the observed behavior regardless of the choice of J. The discrepancy is too large to be explained by the partial delocalization of the Cr^{3+} spins. The most obvious explanation is a magnetocrystalline interaction which favors spin alignment along the c axis. This interaction presumably arises from spin-orbit coupling in "excited" (nonionic) configurations of the Cr^{3+} ion in the weak trigonal component of the $CrCl_3$ crystal field. In ferromagnetic $CrBr_3$ (whose structure differs from that of $CrCl_3$ only in the stacking arrangement of the "sandwiches") the spins are aligned along the c axis.[18,19] Since the dipolar anisotropy makes (001) an easy plane the presence of magnetocrystalline anisotropy is clearly indicated. However, whereas in $CrBr_3$ the single-ion anisotropy energy is larger than the long-range dipolar energy the situation must be reversed in $CrCl_3$. This shift in the balance between the two opposing interactions is in the expected direction because $CrBr_3$ is less ionic than $CrCl_3$ (resulting in greater spin-orbit coupling) and has slightly larger lattice constants (which contributes to a smaller dipolar energy). The effect of the magnetocrystalline anisotropy is easily included in our dipole model as a term $D(S^y)^2$. The necessary corrections are given in Appendix II. Applying the resulting model to our data gives a zero-

[17] J. F. Dillon, in Proceedings of the Conference on Magnetic and Electric Resonance and Relaxation, Eindhoven, 1962 (unpublished).

[18] I. Tsubokawa, J. Phys. Soc. Japan **15**, 1664 (1960).

[19] J. F. Dillon, Suppl. J. Appl. Phys. **33**, 1191 (1962).

field fit for

$$J/k=4.52\pm0.05^\circ\mathrm{K},$$
$$DS/g\beta=-2000\mp100\ \mathrm{Oe}. \quad (18)$$

The reduction of $M(0)$ from its satuation value is again only $\sim0.01\%$. We note that the reduction of the total anisotropy by the single-ion term inferred from the sublattice magnetization data is in line with the small value of the anisotropy inferred by other authors. We also note that the magnitude of the intralayer-exchange constant determined by fitting spin-wave theory to the observed magnetization is fairly insensitive to the exact form of the anisotropy. We believe, therefore, that a value of $4.52\pm0.05^\circ$K represents an accurate determination of J/k within the framework of the Heisenberg exchange model. This is in contrast to the estimate obtained from the molecular field approximation (7) which gives a much smaller value.

IV. INTENSITY ENHANCEMENT

In zero-external field the observation of the Cr^{53} nuclear resonance is presumably made possible by an enhancement mechanism which depends on a rotation of the directions of sublattice magnetization under the influence of the driving field. This rotation produces an oscillatory transverse field at the nucleus which may greatly exceed the applied rf field. The enhancement is similar to the domain rotation mechanism observed in ferromagnets.[20] In $CrCl_3$ the domains consist of the two-dimensional ferromagnetic layers; the restoring force is provided by the antiferromagnetic interlayer interaction. Therefore, the enhancement factor is

$$G=H_{\mathrm{hfs}}/2H_{\mathrm{ex}}, \quad (19)$$

where the interlayer exchange field H_{ex} is given by Eq. (9) as 1450 Oe. Substitution of $H_{\mathrm{hfs}}=2.63\times10^5$ Oe and averaging over all directions in the basal plane gives $G_{(\mathrm{av})}\approx57$. This value is consistent with observations.

In the presence of a weak external magnetic field we have found that the resonance intensity is remarkably enhanced over its zero-field value.[21] This observation is consistent with a model of increased domain rotation which results from the torque exerted by the rf field on the net field-induced magnetization; i.e., the two sublattices rotate in phase under the influence of the rf field rather than in opposition as is required in zero external field. We postulate a weak anisotropy acting on the spins in the (001) plane. This anisotropy might arise from slight distortions of the chlorine octahedra. In weak external fields the rotation of the magnetization is damped largely by this anisotropy. Thus, the enhancement increases with increasing field (since the magnetization increases while the restoring force remains constant) until the external field overcomes the anisotropy and the net magnetization turns parallel to the applied field (i.e., spin-flopping occurs). Beyond that point the external field provides most of the restoring force and the enhancement quickly decreases again. In terms of this static model with the notation of Fig. 4 we can write the energy of the system in the presence of a field of arbitrary direction in the (001) plane as

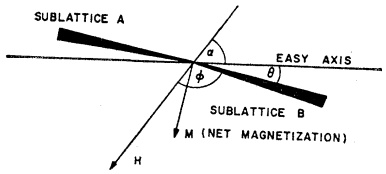

FIG. 4. Schematic representation of $CrCl_3$ spin system in (001) plane in an external magnetic field.

$$E=-\tfrac{1}{2}\chi_\perp H^2\sin^2\phi-\tfrac{1}{2}\chi_{\parallel}H^2\cos^2\phi+K\sin^2 3\theta. \quad (20)$$

Here $\chi_\perp$ and $\chi_{\parallel}$ are the volume susceptibilities (we have used a molar volume of $v=53.8$ cm^3/mole), K is the anisotropy constant, and the angular dependence is of lowest order consistent with the symmetry of the lattice. The displacement θ from the easy axis is determined by minimizing the energy. We obtain the condition

$$H^2(\chi_\perp-\chi_{\parallel})\sin 2(\alpha+\theta)-6K\sin 6\theta=0. \quad (21)$$

We now consider the angular displacement of the system by the driving field (H_1) for two different orientations of H_1 with respect to H. With $H_1\perp H$ the enhancement can be shown to be proportional to $(1/H)\partial\theta/\partial\alpha$; with $H_1\|H$ it is proportional to $\partial\theta/\partial H$. From (21) and the relationship $\alpha+\theta+\phi=\pi$ we then obtain

$H_1\perp H$:

$$G_\perp=\frac{H_{\mathrm{hfs}}H(\chi_\perp-\chi_{\parallel})\cos 2\phi}{18K\cos 6\theta-H^2(\chi_\perp-\chi_{\parallel})\cos 2\phi}; \quad (22)$$

$H_1\|H$:

$$G_{\parallel}=\frac{H_{\mathrm{hfs}}H(\chi_\perp-\chi_{\parallel})\sin 2\phi}{18K\cos 6\theta-H^2(\chi_\perp-\chi_{\parallel})\cos 2\phi}. \quad (23)$$

In both cases the expressions demonstrate the linear dependence of G on H for weak fields and the inverse dependence for strong fields. The dependence of G on ϕ will be discussed in the next section.

The expressions (22) and (23) are only valid in fields too weak to produce spin flopping. Above this point the magnetization M lies parallel to H and remains so as H rotates. The enhancement factors are then given by

$$G_\perp=H_{\mathrm{hfs}}/H, \quad (24)$$
$$G_{\parallel}=0. \quad (25)$$

From (24) it can be seen that nuclear resonance absorption by magnetic ions in antiferromagnetic systems should be strongly enhanced in external fields above the spin-flopping transition as long as this transition occurs in fields sufficiently weaker than the hyperfine field. For example, the Cu resonance in $CuCl_2$

[20] A. C. Gossard and A. M. Portis, Phys. Rev. Letters 3, 164 (1959).
[21] A. Narath, Bull. Am. Phys. Soc. 7, 481 (1962).

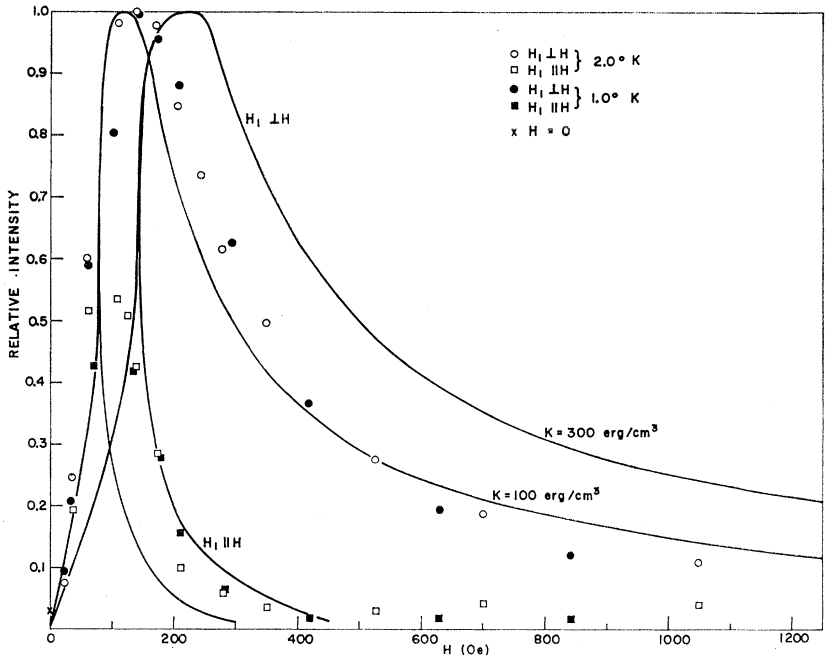

FIG. 5. Plot of normalized field-enhanced intensities of the Cr^{53} NMR in $CrCl_3$ at 1 and 2°K. Solid curves are calculated from the enhancement model given in text.

$\cdot 2H_2O$ above[22] 7000 Oe and the Co resonance in $CoCl_2$ above[23] 2000 Oe should exhibit this effect. Since the steady field is at right angles to the directions of sublattice magnetization only a small shift in the resonance frequency from the zero-field value is expected.

In order to compare the predictions of the enhancement model with experiment, numerical calculations were carried out to obtain a value for the average enhancement appropriate to our randomly oriented samples. The value of $\chi_{\parallel}$ obtained in Sec. V was used. The calculations were programmed for the Sandia Laboratory CDC-1604 digital computer. For a given orientation of H the value of θ corresponding to the nearest energy minimum was obtained by a trial and error solution of Eq. (21). The perpendicular and parallel enhancements were then calculated from (22) and (23) [or (24) and (25) when necessary]. The calculation was repeated by increasing H in steps of 5 Oe. Each solution of (21) used the value of θ calculated for the preceding cycle as a starting point. The calculation was carried out for 500 values of α evenly spaced between 0 and $\pi/2$ and for fields up to 1400 Oe. The average normalized enhancements are plotted in Fig. 5 for two values of K together with experimental points taken at 2 and 1°K. The measured field values have been corrected for demagnetization effects

$$H(\text{eff})=H(1+N\chi_{\perp})^{-1}\approx 0.70H, \tag{26}$$

where $N=4\pi/3$ is the demagnetizing factor appropriate for the spherical sample used in the measurements. Although the average susceptibility of the polycrystalline samples is not given correctly by $\chi_{\perp}$ for very weak fields, the sensitivity of the experiment does not warrant an attempt to correct for this effect. Comparison of experiment and theory shows satisfactory agreement. From the fit we obtain

$$K=150\pm 50 \text{ erg/cm}^3, \tag{27}$$

corresponding to an anisotropy field in the (001) plane given by

$$H_A'=18K/M=8.7 \text{ Oe}.$$

The calculated maximum average perpendicular enhancement is 1480. Thus, the ratio of maximum field-induced enhancement to the zero-field enhancement is calculated to be 26. The experimental ratio at 2.0°K is 33. It is not certain whether the magnitude of the basal plane anisotropy determined in this experiment is an intrinsic property of antiferromagnetic $CrCl_3$ or whether it contains appreciable contributions from lattice imperfections and domain wall effects. Some of the "pressed flake" samples exhibited anisotropies which were larger than that observed in the spherical sample. In general, however, the results were quite consistent among different samples, suggesting that most of the anisotropy represents an intrinsic property.

In principle, one expects hysteresis effects in the intensities and frequencies observed in our field-effect experiments. These effects would arise from nonrandom population of equivalent domain directions during demagnetization as observed, for example, in $CoCl_2$[23].

[22] J. Van Den Handel, H. M. Gijsman, and N. J. Poulis, Physica **18**, 862 (1952).
[23] M. K. Wilkinson, J. W. Cable, E. O. Wollan, and W. C. Koehler, Phys. Rev. **113**, 497 (1959).

In $CrCl_3$, however, the anisotropy is so small that we have not been able to detect these changes.

The observation of strong enhancements in external fields implies very short spin-lattice relaxation times, since no saturation effects were observed even at the lowest temperature reached in our experiments. This is in agreement with direct measurements of T_1 by transient techniques[24] which gave relaxation times of only a few milliseconds even at 1°K.

V. MAGNETIC FIELD EFFECTS

A magnetic field is found to shift the Cr^{53} resonance frequencies. One expects these shifts to arise from two mechanisms. The first is the direct interaction between the field and the nuclear moment which, in weak fields, produces a shift $\gamma_{Cr^{53}} H \cos\phi$. Here $\gamma_{Cr^{53}}$ is the appropriate gyromagnetic ratio (0.2406 kc/sec-Oe). The second mechanism arises from the field dependence of the sublattice magnetization. Any field-induced change in the sublattice magnetization is, of course, reflected in a proportional change in the hyperfine field and, hence, results in a frequency shift of the nuclear resonance. These two effects are easily distinguished from one another. The direct interaction has no temperature dependence except for slight changes in demagnetizing effects. The field dependence of the sublattice magnetization, on the other hand, is a function of temperature since the parallel magnetic susceptibility ($\chi_{\parallel}$) nearly vanishes at $T=0$°K. Another difference between the two interactions is the direction of the shift. The hyperfine field at the chromium nucleus in $CrCl_3$ is found to be negative with respect to the direction of magnetization. (The evidence for this is presented later in this section.) Hence, as a result of the direct interaction the field at the nucleus tends to decrease in an increasing external field applied along the sublattice magnetization. The sublattice magnetization itself, however, increases and hence produces an increase in the hyperfine field. The net shift of the resonance depends, therefore, on the relative magnitude of the two opposing effects.

A unique feature of a two-dimensional ferromagnetic spin system, in the presence of a weak anisotropy field, is the prediction of a large parallel susceptibility. This is most easily seen in the long-wave limit [Eq. (5)]. The magnetization is seen to diverge at any finite temperature unless an effective field exists. This strong field dependence is not found in three-dimensional systems since they are stable even in the absence of anisotropy. A direct measurement of $\chi_{\parallel}$ is difficult in $CrCl_3$ because of the weak field at which spin-flopping occurs. However, the field-induced enhancement mechanism discussed in the preceding section makes it possible to determine $\chi_{\parallel}$ in our polycrystalline samples by means of nuclear resonance techniques. We note that in weak fields the enhancement factor depends on the angle ϕ between the directions of H and the sublattice magnetizations. For the special case of $G_{\parallel}$ (i.e., $H_1 \| H$) the enhancement is a maximum for $\phi=45°$ and is zero for $\phi=0$ and 90°. For this field configuration the main resonance intensity is, therefore, expected to arise from domains for which ϕ is near 45°. The two magnetic sublattices for these antiferromagnetic domains will experience magnetic fields with appreciable components parallel and antiparallel to the directions of sublattice magnetization, respectively. The selective excitation predicted by the enhancement model should, therefore, result in a splitting of the nuclear resonance. We report here measurements of this effect on two different samples: (1) the spherical specimen which was used in the enhancement studies; (2) a "pressed flake" specimen which exhibited a particularly high spin-flopping field ($\sim$225 Oe). Figure 6 shows observed spectra ($H_1 \| H$) of the Cr^{53} quadrupole triplet at 4.00°K for the "pressed flake" sample. The field dependence of the sublattice magnetization is reflected in a change in the hyperfine field resulting in a splitting of the resonance given by

$$\Delta\nu_{T,H} = 2H(\eta_{T,H} - \gamma_{Cr^{53}})\cos\phi\,, \qquad (28)$$

where $\eta_{T,H}$ is the temperature and field-dependent change in the hyperfine field per unit change in magnetic-field strength. Here we have only considered the

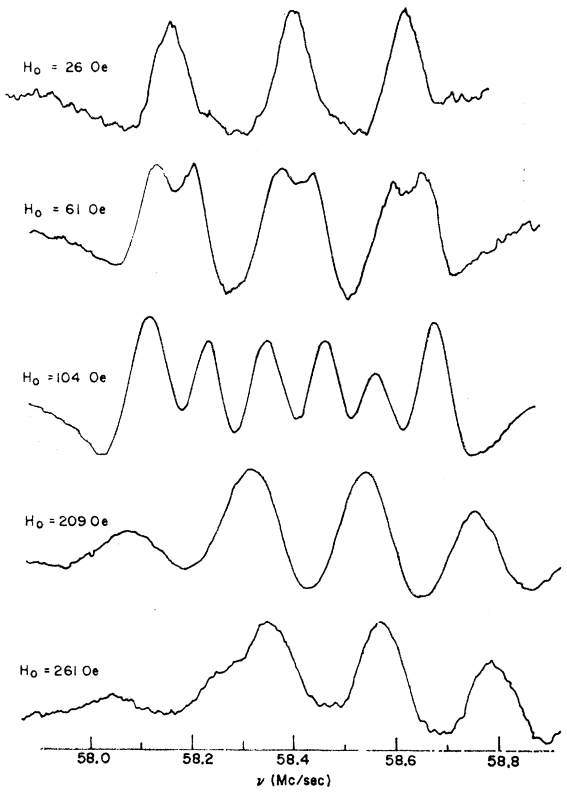

FIG. 6. Second-derivative tracings of Cr^{53} nuclear resonances in $CrCl_3$ with $H_1 \| H$ at 4.00°K.

[24] A. T. Fromhold and A. Narath (to be published).

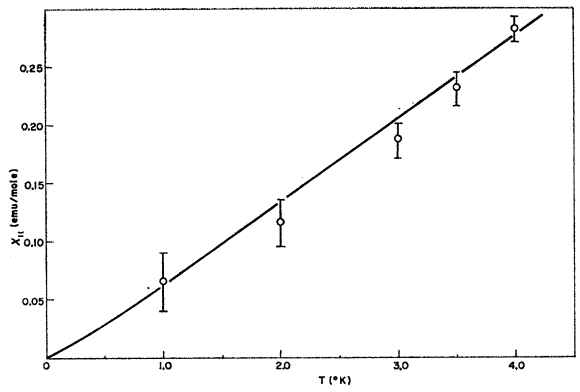

FIG. 7. Plot of the temperature dependence of the parallel magnetic susceptibility of $CrCl_3$ derived from observed splittings of the Cr^{53} NMR in an external magnetic field with $H_1 \| H$. Solid curve is the susceptibility calculated from the two-dimensional ferromagnetic spin-wave model with explicit treatment of intralayer dipole-dipole interactions and the single-ion anisotropy, $D(S^y)^2$.

effect of the field component along the directions of sublattice magnetization. The molar susceptibility χ_{II} is obtained from $\eta_{T,H}$ by

$$\chi_{II}=\eta_{T,H}M_s/\nu(0)\,, \tag{29}$$

where M_s is the saturation magnetization, which in $CrCl_3$ corresponds to $3\mu_B$ (16,756 emu/mole). At 4.00°K we find $\Delta\nu_{T,H}=234$ kc/sec for a field strength of 200 Oe. Using (28) and (29) with $\phi=45°$ we obtain $\chi_{II}=0.28\pm0.01$ emu/mole at this temperature. We have calculated χ_{II} from the two-dimensional effective-field and dipole spin-wave models by including a small field H in H_A and using the constants given in (6) and (18), respectively. The results at 4.00°K are 0.227 and 0.276 emu/mole, respectively. The temperature dependence of the parallel magnetic susceptibility calculated from the observed splittings ($H_1 \| H$) together with results of calculations based on the dipole model are shown in Fig. 7. The decrease in magnitude of the observed splittings with decreasing temperature confirms that the observed shifts are indeed dominated by changes in the sublattice magnetization. Although the close agreement between theory and experiment in the case of the dipole model may be somewhat fortuitous it is worth noting that even the simple effective-field model results in a rather satisfactory fit. The large value of χ_{II} in $CrCl_3$ at 4.00°K compares with $\chi_{II}=0.0036$ in[25] MnF_2 at a comparable temperature ($T/T_N=0.236$).

The perpendicular field configuration ($H_1 \perp H$) leads to different observations. According to Eq. (22), enhancement maxima occur for $\phi=0$ and 90°. The $\phi=0°$ domains should exhibit resonance splittings but the $\phi=90°$ domains should not, since for the latter both sublattices experience the same field. However, the enhancement calculations described earlier show that the intensity becomes dominated by the $\phi=90°$ domains before an observable splitting of each line is possible. Therefore, we expect severe line broadening but no observable splittings. This is in agreement with observations.

The results of our weak field measurements at 4.00°K are summarized in Fig. 8. Demagnetization corrections have again been applied to the data for the spherical sample. The "pressed flake" sample was in the shape of a long rod (magnetized along the major axis) and no corrections were deemed necessary. The agreement between the two sets of data makes this procedure reasonable. The spin-flopping transitions are clearly indicated for the two samples. In both cases, the transition fields determined from the frequency shifts are in excellent agreement with the maxima in the parallel enhancement (Fig. 5). These maxima occur at lower fields than the critical field $H_C=(H_A'^2+2H_{ex}H_A')^{1/2}$ because we are observing $\phi\cong45°$ (not $\phi=0°$) domains in our polycrystalline samples. In the case of the spherical sample the enhancement calculations predict a maximum splitting (for $H_1 \| H$) at $H=90$ Oe in good agreement with observation. The calculation was carried out in the following way. For each value of H an intensity weighted average of all ϕ was calculated. The splitting calculated from the dipole model for this value was presumed to correspond to the observed splitting. For weak fields the average calculated value of ϕ is 45°; near $H=90$ Oe it begins to increase and the resulting decrease in the parallel field component quickly overcomes the effect of increasing the external field. Above the spin-flopping transition the frequencies (but not the intensities) for the perpendicular and parallel configurations are indistinguishable.

In addition to being broadened, the resonances observed with $H_1 \perp H$ also exhibit frequency shifts in the external field. This can be seen in Fig. 8 for weak fields at 4°K and in Fig. 9 for stronger fields at several

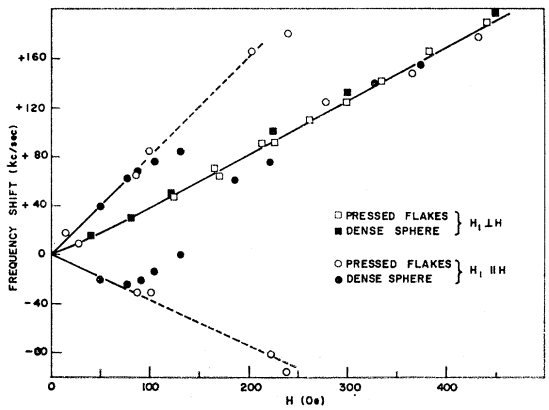

FIG. 8. Plot of observed weak-field frequency shifts of the Cr^{53} NMR in $CrCl_3$ at 4.00°K for $H_1 \| H$ and $H_1 \perp H$. Solid curves are smooth fits to the data.

[25] J. W. Stout and M. Griffel, J. Chem. Phys. **18**, 1455 (1950).

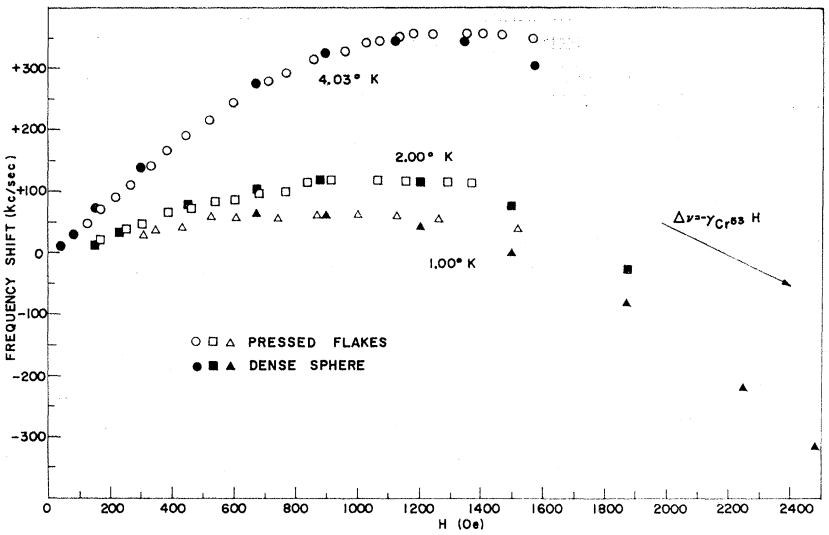

FIG. 9. Plot of the frequency shifts of the Cr^{53} NMR in $CrCl_3$ in an external magnetic field with $H_1 \perp H$.

temperatures. Even the weak field $H_1 \| H$ data demonstrate this effect. Since $\phi = 45°$ in this case, there is in addition to the parallel field component a perpendicular component. This component manifests itself by an increase in the average frequency of the high- and low-frequency branches of the split resonance. Although we have been unable to account for these observations quantitatively we can give a qualitative explanation or the measured shifts. The weak-field slope of frequency versus field is strongly temperature-dependent. It appears, therefore, that the shifts are caused by changes in sublattice magnetization. The initial slope is due to the combined effects of the parallel and perpendicular field components on the spin system. With increasing field the antiferromagnetic sublattices gradually turn parallel to each other and the parallel field component becomes increasingly more important compared to the decreasing perpendicular component. However, the parallel susceptibility decreases with increasing field as can be seen from Eq. (5). This leads to a reduction in slope of the frequency versus field plot. The experimental observation that the resonance frequencies reach a maximum and then decrease again indicates that the hyperfine field is negative. As the susceptibility saturates, the direct interaction between field and nuclear moment becomes gradually dominant and causes a reduction in the net field at the nucleus. Above 2 kOe the frequencies for the spherical sample decrease somewhat more rapidly than expected from the magnitude of the Cr^{53} moment. This suggests that this sample approaches magnetic saturation at slightly lower fields than expected from the measured perpendicular susceptibility. In other words, we have applied demagnetization corrections which are too large above 2 kOe. This conclusion is in agreement with the observation that the "pressed-flake" data (for which no demagnetization corrections were required) do not fall off as quickly at higher field strengths even though they agree with the data for the spherical sample at lower fields. The negative hyperfine field which we have determined for $CrCl_3$ is consistent with the negative hyperfine field observed in $CrBr_3$.

The zero-field line widths for the spherical sample vary smoothly from 90 kc/sec at 4.0°K to 25 kc/sec at 0.4°K. These widths (at least at the higher temperatures) are primarily due to sample inhomogeneities (domain structures, etc.). This is confirmed by transient measurements.[24] The application of a magnetic field at 4°K initially broadens the resonance; above the spin-flopping transition, narrowing sets in until the line width reaches 25 kc/sec at 2 kOe. This narrowing is caused by an increase in the magnetic homogeneity under the influence of the field. The narrowing effect of the field decreases with decreasing temperature; at 0.4°K no change is observed. This is to be expected since variations in the effective anisotropy have a much greater influence on the sublattice magnetization at high temperatures than at low temperatures. The line widths for the "pressed-flake" samples are somewhat greater than for the spherical sample.

VI. IMPURITY EFFECTS

The frequencies of the Cr^{53} resonance are not significantly affected by small concentrations of chemical impurities. Some of the commercial $CrCl_3$ samples contained 0.6% Fe, presumably as a substitutional impurity, without producing measurable shifts in the observed frequencies. However, the observed spectra are strongly influenced by crystallographic imperfections. Because of the weak forces which bind the $CrCl_3$ sandwiches together it is easy to produce stacking dislocations. These manifest themselves in broadening and slight shifts of the resonances, expecially at the

higher temperatures. In addition, all of our powder samples displayed an extra resonance in the form of a badly distorted quadrupole triplet. This resonance was observed 1.18 Mc/sec above the normal resonance at 4.0°K. On decreasing the temperature this separation decreases linearly. Although measurements below 1.2°K were not carried out because of interference between the two sets of resonances, extrapolation of the high-temperature data suggests that the separation vanishes at 0°K. The extraneous resonances saturate easily and decrease in intensity in external fields without being initially enhanced as is the case for the normal resonances. This behavior suggests that these resonances are due to a component with a net magnetic moment. No normal resonance was observed in a sample which had been rapidly sublimed so as to yield particle sizes no larger than 1μ. Instead, a triplet with broadened satellites was observed at the higher frequency. This line shape is indicative of inhomogeneity in the electric-field gradient at the Cr^{3+} sites due to crystallographic imperfections. On the other hand, the spherical specimen for which we have presented data in this paper had no detectable resonance at the higher frequency. We have also found that grinding of previously good samples eliminates the normal resonance and substitutes a complex spectrum centered at the position of the extraneous resonance. It is not clear why the imperfect component should exhibit a higher sublattice magnetization than the normal component. Comparison of the data for the extraneous absorption with the simple spin-wave model suggests that the J's are the same for the two components but that the impurity component has a higher effective anisotropy. The presence of a net moment in imperfect samples would account for the occasional observation of magnetic-hysteresis effects in $CrCl_3$.[26]

Another unexplained feature of our $CrCl_3$ measurements is a slight discrepancy between the zero-field resonance frequencies and those observed under field enhancement. The field-enhanced frequencies consistently extrapolate to a zero-field value about 40 kc/sec lower than the observed zero-field value regardless of temperature. At 0.4°K this effect can be resolved because of the narrow linewidths. In an external field ($H_1 \| H$) of about 10 Oe the field-enhanced resonance and the "zero-field" resonance are observed separated by $\sim$40 kc/sec; on increasing the field the former quickly increases in intensity while the latter slowly diminishes.

VII. SUMMARY

The low-temperature sublattice magnetization of antiferromagnetic $CrCl_3$, as determined by zero-field nuclear resonance measurements, provides an interesting application of the isotropic Heisenberg exchange model in the spin-wave approximation. $CrCl_3$ is an ideal system for such a study because the appropriate spin Hamiltonian is sufficiently simple to permit a fairly rigorous analysis of the data. The salient features of the model which we have investigated are an isotropic, ferromagnetic, intralayer-exchange interaction restricted to nearest neighbors and an antiferromagnetic interlayer interaction which is treated as an effective anisotropy field. In addition, both long-range magnetic-dipolar and single-ion magnetocrystalline interactions are required to fit the sublattice magnetization data. We have shown that this model gives a quantitative explanation for the two unique properties of the $CrCl_3$ spin system: (1) the strong, nearly linear temperature dependence of the sublattice magnetization, and (2) the unusually large parallel magnetic susceptibility. In Table I we have summarized the $CrCl_3$ interaction constants which have been discussed in this paper.

TABLE I. Interaction constants of the $CrCl_3$ spin system.

$J_z/k = 13.56 \pm 0.15$°K
$J_{Lz_L}/k = -0.065$°K
$H_D(001) = 2254$ Oe
$DS/g\beta = -2000 \pm 100$ Oe
$K(001) = 150 \pm 50$ ergs/cm^3
$\chi_\perp(T = 4.0°\text{K})$[8] $= 5.5$ emu/mole
$\chi_{\|}(T = 4.0°\text{K}) = 0.28 \pm 0.01$ emu/mole
H_{hfs} (corrected for $-H_D$ at $T = 0°\text{K}) = 2.6540 \times 10^5$ Oe

ACKNOWLEDGMENTS

The author acknowledges with great pleasure many helpful and stimulating discussions with Dr. D. C. Wallace and wishes to express his appreciation to David C. Barham for technical assistance. An illuminating discussion with Professor A. M. Portis is gratefully acknowledged. Thanks is also due to Dr. A. Yoshimori for making a preprint of his work available before publication.

APPENDIX I

We consider the Hamiltonian of Eq. (1) with the addition of a dipole-dipole interaction term given by

$$\mathcal{H}_D = -\tfrac{1}{2} \sum_{ii',pp'} \frac{3(g\beta)^2}{|\mathbf{r}_{ip} - \mathbf{r}_{i'p'}|^5} \sum_{q=-2}^{+2} (-1)^q \{\mathbf{S}_{ip}, \mathbf{S}_{i'p'}\}_2^q \times \{(\mathbf{r}_{ip} - \mathbf{r}_{i'p'})^2\}_2^{-q}, \quad (30)$$

where $\{\ \}_2$ denotes the general second-rank irreducible tensors constructed from the appropriate vectors. In the following we shall simplify the notation for the lattice vectors: We let

$$\mathbf{r} = \mathbf{r}_{ip} - \mathbf{r}_{i'p'}, \quad \mathbf{r}_0 = \mathbf{r}_{ip} - \mathbf{r}_{i'p}, \quad (31)$$

[26] W. J. De Haas, B. H. Schultz, and J. Koolhaas, Physica 7, 57 (1940).

and similarly for x, y, z. We introduce creation ($a^\dagger$) and annihilation (a) operators in the usual way and invoke the low-temperature spin-wave approximation; i.e., we retain only terms bilinear or quadratic in the spin-wave operators and let $(1-a^\dagger a/2S)^{1/2}=1$. After transforming to a lattice-wave representation we obtain

$$\begin{aligned}\mathcal{H}&=\mathcal{H}_0+\sum_{\mathbf{k},pp'}(A_{\mathbf{k},pp'}a_{\mathbf{k}p}{}^\dagger a_{\mathbf{k}p'}+B_{\mathbf{k},pp'}a_{\mathbf{k}p}a_{-\mathbf{k}p'}\\&\qquad+B_{\mathbf{k},pp'}{}^*a_{\mathbf{k}p}{}^\dagger a_{-\mathbf{k}p'}{}^\dagger),\quad(32)\\\mathcal{H}_0&=-2NS(g\beta H_A+JSz)\\&\qquad-\tfrac{1}{2}(g\beta)^2NS^2\textstyle\sum_{i,pp'}{}'(3z^2-r^2)r^{-5},\end{aligned}$$

and

$$\begin{aligned}A_{\mathbf{k},pp'}&=g\beta(H_A+H_D)+2JSz+\tfrac{1}{2}(g\beta)^2\\&\qquad\times S\textstyle\sum_i{}'(3z_0{}^2-r_0{}^2)r_0{}^{-5}\cos\mathbf{k}\cdot\mathbf{r}_0\quad\text{for}\quad p=p'\\&=-2JS\textstyle\sum_i{}^{\text{n.n.}}\exp(-i\mathbf{k}\cdot\mathbf{r}_0)+\tfrac{1}{2}(g\beta)^2\\&\qquad\times S\textstyle\sum_i{}'(3z^2-r^2)r^{-5}\exp(-i\mathbf{k}\cdot\mathbf{r}_0)\quad\text{for}\quad p\neq p'\\B_{\mathbf{k},pp'}&=-(3/4)(g\beta)^2S\textstyle\sum_i{}'(x-iy)^2r^{-5}\exp(-i\mathbf{k}\cdot\mathbf{r}_0),\end{aligned}$$

where the nearest neighbor sum $\sum_i{}^{\text{n.n.}}$ is restricted to terms $\mathbf{r}_0$ which connect the lattice points (i',p) and (i,p) corresponding to the exchange interaction $J_{i'i,pp'}$. We note that $A_{\mathbf{k},pp}$ contains in addition to H_A the complete lattice dipole sum

$$H_D=g\beta S\textstyle\sum_{i,p'}{}'(3z^2-r^2)r^{-5}.\quad(33)$$

Difficulty in finding the eigenvalues of $\mathcal{H}$ rests primarily in the non-Hermitian form of B. For our two-dimensional model a great simplification occurs since we can put $y=0$. The B matrices are now Hermitian. We shall restrict ourselves to the case in which the dipole-dipole interaction is smaller than the intralayer exchange interaction, but does not vanish. The solution to the resulting problem is obtained by the following series of transformations.

(1) We define

$$a_{\mathbf{k}p}=\textstyle\sum_s V_{\mathbf{k},sp}a_{\mathbf{k}s},\quad a_{\mathbf{k}p}{}^\dagger=\sum_s V_{\mathbf{k},sp}{}^*a_{\mathbf{k}s}{}^\dagger,\quad(34)$$

where the vectors $\mathbf{V}$ are determined from the secular equation

$$\textstyle\sum_{p'}A_{\mathbf{k},pp'}V_{\mathbf{k},sp'}=\lambda_{\mathbf{k}s}V_{\mathbf{k},sp};\quad\lambda_{\mathbf{k}s}=\lambda_{-\mathbf{k}s}.\quad(35)$$

Since the $\lambda_{\mathbf{k}s}$ are real we can choose

$$V_{\mathbf{k},sp}{}^*=V_{-\mathbf{k},sp}.$$

Also, since A is Hermitian, the vectors are found to satisfy orthonormality and completeness relations. The transformed Hamiltonian can now be written as

$$\begin{aligned}\mathcal{H}&=\mathcal{H}_0+\textstyle\sum_{\mathbf{k}s}\lambda_{\mathbf{k}s}a_{\mathbf{k}s}{}^\dagger a_{\mathbf{k}s}\\&\qquad+\textstyle\sum_{\mathbf{k},ss'}(\rho_{\mathbf{k},ss'}a_{\mathbf{k}s}a_{-\mathbf{k}s'}+\rho_{\mathbf{k},ss'}{}^*a_{\mathbf{k}s}{}^\dagger a_{-\mathbf{k}s'}{}^\dagger),\quad(36)\end{aligned}$$

where

$$\begin{aligned}\rho_{\mathbf{k},ss'}&=\textstyle\sum_{pp'}B_{\mathbf{k},pp'}V_{\mathbf{k},sp}V_{-\mathbf{k},s'p'}\\\rho_{\mathbf{k},ss'}&=\rho_{\mathbf{k},s's}{}^*=\rho_{-\mathbf{k},s's}\\[a_{\mathbf{k}s},a_{\mathbf{k}'s'}{}^\dagger]&=\delta_{\mathbf{k}\mathbf{k}'}\delta_{ss'}.\end{aligned}$$

(2) We can now remove the interactions between $\mathbf{k}$ and $-\mathbf{k}$. We introduce appropriate transformations for positive ($k^z>0$) and negative ($k^z<0$) half-spaces of $\mathbf{k}$.

$$\begin{aligned}&k^z>0&&k^z<0\\a_{\mathbf{k}s}&=2^{-\frac{1}{2}}e^{\pm i\phi\mathbf{k}}(b_{\mathbf{k}s}+b_{-\mathbf{k}s}),&&=2^{-\frac{1}{2}}e^{\mp i\phi\mathbf{k}}(b_{\mathbf{k}s}-b_{-\mathbf{k}s})\\a_{\mathbf{k}s}{}^\dagger&=2^{-\frac{1}{2}}e^{\mp i\phi\mathbf{k}}(b_{\mathbf{k}s}{}^\dagger+b_{-\mathbf{k}s}{}^\dagger),&&=2^{-\frac{1}{2}}e^{\pm i\phi\mathbf{k}}(b_{\mathbf{k}s}{}^\dagger-b_{-\mathbf{k}s}{}^\dagger)\\a_{-\mathbf{k}s}&=2^{-\frac{1}{2}}e^{\mp i\phi\mathbf{k}}(b_{\mathbf{k}s}-b_{-\mathbf{k}s}),&&=2^{-\frac{1}{2}}e^{\pm i\phi\mathbf{k}}(b_{\mathbf{k}s}+b_{-\mathbf{k}s})\\a_{-\mathbf{k}s}{}^\dagger&=2^{-\frac{1}{2}}e^{\pm i\phi\mathbf{k}}(b_{\mathbf{k}s}{}^\dagger-b_{-\mathbf{k}s}{}^\dagger),&&=2^{-\frac{1}{2}}e^{\mp i\phi\mathbf{k}}(b_{\mathbf{k}s}{}^\dagger+b_{-\mathbf{k}s}{}^\dagger).\end{aligned}\quad(37)$$

The upper sign is understood for $s=1$ and the lower sign for $s=2$. The phase angles are defined by

$$\rho_{\mathbf{k},12}=|\rho_{\mathbf{k},12}|\exp(-2i\phi_{\mathbf{k}}).$$

The transformed Hamiltonian becomes

$$\begin{aligned}\mathcal{H}&=\mathcal{H}_0+\textstyle\sum_{k^z>0,s}\lambda_{\mathbf{k}s}(b_{\mathbf{k}s}{}^\dagger b_{\mathbf{k}s}+b_{-\mathbf{k}s}{}^\dagger b_{-\mathbf{k}s})\\&\qquad+\textstyle\sum_{k^z>0,ss'}\gamma_{\mathbf{k},ss'}[(b_{\mathbf{k}s}b_{\mathbf{k}s'}+b_{\mathbf{k}s}{}^\dagger b_{\mathbf{k}s'}{}^\dagger)\\&\qquad-(b_{-\mathbf{k}s}b_{-\mathbf{k}s'}+b_{-\mathbf{k}s}{}^\dagger b_{-\mathbf{k}s'}{}^\dagger)],\quad(38)\end{aligned}$$

with

$$\begin{aligned}\gamma_{\mathbf{k},ss'}&=\gamma_{\mathbf{k},s's}=|\rho_{\mathbf{k},ss'}|,\\\gamma_{\mathbf{k},ss'}&=\gamma_{-\mathbf{k},ss'}.\end{aligned}$$

The transformation leading to $\lambda_{\mathbf{k}s}$ and $\gamma_{\mathbf{k},ss'}$ can be carried out explicitly. We find

$$\begin{aligned}\lambda_{\mathbf{k}1}&=A_{\mathbf{k},11}+(u_{\mathbf{k}}\cos x_{\mathbf{k}}+v_{\mathbf{k}}\sin x_{\mathbf{k}}),\\\lambda_{\mathbf{k}2}&=A_{\mathbf{k},11}-(u_{\mathbf{k}}\cos x_{\mathbf{k}}+v_{\mathbf{k}}\sin x_{\mathbf{k}}),\\\gamma_{\mathbf{k},11}&=B_{\mathbf{k},11}+(u_{\mathbf{k}}{}'\cos x_{\mathbf{k}}+v_{\mathbf{k}}{}'\sin x_{\mathbf{k}}),\\\gamma_{\mathbf{k},22}&=B_{\mathbf{k},11}-(u_{\mathbf{k}}{}'\cos x_{\mathbf{k}}+v_{\mathbf{k}}{}'\sin x_{\mathbf{k}}),\\\gamma_{\mathbf{k},12}&=|(u_{\mathbf{k}}{}'\sin x_{\mathbf{k}}-v_{\mathbf{k}}{}'\cos x_{\mathbf{k}})|,\end{aligned}\quad(39)$$

where

$$\begin{aligned}u_{\mathbf{k}}&=\text{Re}(A_{\mathbf{k},21}),&u_{\mathbf{k}}{}'&=\text{Re}(B_{\mathbf{k},21}),\\v_{\mathbf{k}}&=\text{Im}(A_{\mathbf{k},21}),&v_{\mathbf{k}}{}'&=\text{Im}(B_{\mathbf{k},21}),\\x_{\mathbf{k}}&=\tan^{-1}(v_{\mathbf{k}}/u_{\mathbf{k}}).\end{aligned}$$

(3) It is convenient at this point to transform to harmonic oscillator coordinates in the following way:

$$\begin{aligned}b_{\mathbf{k}1}&=\tfrac{1}{2}[(\alpha_{\mathbf{k}}q_{\mathbf{k}1}+i\beta_{\mathbf{k}}p_{\mathbf{k}1})+(q_{\mathbf{k}2}+ip_{\mathbf{k}2})],\\b_{\mathbf{k}1}{}^\dagger&=\tfrac{1}{2}[(\alpha_{\mathbf{k}}q_{\mathbf{k}1}-i\beta_{\mathbf{k}}p_{\mathbf{k}1})+(q_{\mathbf{k}2}-ip_{\mathbf{k}2})],\\b_{\mathbf{k}2}&=\tfrac{1}{2}[(q_{\mathbf{k}1}+ip_{\mathbf{k}1})-(\beta_{\mathbf{k}}q_{\mathbf{k}2}+i\alpha_{\mathbf{k}}p_{\mathbf{k}2})],\\b_{\mathbf{k}2}{}^\dagger&=\tfrac{1}{2}[(q_{\mathbf{k}1}-ip_{\mathbf{k}1})-(\beta_{\mathbf{k}}q_{\mathbf{k}2}-i\alpha_{\mathbf{k}}p_{\mathbf{k}2})],\end{aligned}\quad(40)$$

and similarly for the $-\mathbf{k}$ terms. The commutators are

$$\begin{aligned}[p_{\mathbf{k}t},p_{\mathbf{k}'t'}]&=[q_{\mathbf{k}t},q_{\mathbf{k}'t'}]=0,\\[p_{\mathbf{k}t},q_{\mathbf{k}'t'}]&=-i\delta_{\mathbf{k}\mathbf{k}'}\delta_{tt'}2(1+\alpha_{\mathbf{k}}\beta_{\mathbf{k}})^{-1},\end{aligned}$$

and the transformation coefficients are taken to be

$$\begin{aligned}\alpha_{\mathbf{k}}&=L_{\mathbf{k}}+(L_{\mathbf{k}}{}^2+M_{\mathbf{k}})^{1/2}=-\beta_{-\mathbf{k}},\\\beta_{\mathbf{k}}&=\alpha_{\mathbf{k}}M_{\mathbf{k}}{}^{-1}=-\alpha_{-\mathbf{k}},\end{aligned}\quad(41)$$

where

$$\begin{aligned}M_{\mathbf{k}}&=\frac{-|A_{\mathbf{k},12}|+\gamma_{\mathbf{k},11}+\gamma_{\mathbf{k},22}}{|A_{\mathbf{k},12}|+\gamma_{\mathbf{k},11}+\gamma_{\mathbf{k},22}},\\L_{\mathbf{k}}&=(4\gamma_{\mathbf{k},12})^{-1}[(\lambda_{\mathbf{k}1}+2\gamma_{\mathbf{k},11})M_{\mathbf{k}}-(\lambda_{\mathbf{k}2}+2\gamma_{\mathbf{k},22})].\end{aligned}\quad(42)$$

Then

$$\mathcal{H}=\mathcal{H}_0+\sum_{k^z>0}(Q_{k1}q_{k1}^2+P_{k1}p_{k1}^2+Q_{k2}q_{k2}^2+P_{k2}p_{k2}^2 +P_{k1}q_{-k1}^2+Q_{k1}p_{-k1}^2+P_{-k2}q_{-k2}^2 +Q_{k2}p_{-k2}^2+2R_k), \quad (43)$$

where

$$\begin{aligned}
R_k&=-\tfrac{1}{2}(\lambda_{k1}+\lambda_{k2}),\\
Q_{k1}&=\tfrac{1}{4}[\alpha_k^2(\lambda_{k1}+2\gamma_{k,11})+(\lambda_{k2}+2\gamma_{k,22})]+\alpha_k\gamma_{k,12},\\
P_{k1}&=\tfrac{1}{4}[\beta_k^2(\lambda_{k1}-2\gamma_{k,11})+(\lambda_{k2}-2\gamma_{k,22})]-\beta_k\gamma_{k,12},\\
Q_{k2}&=\tfrac{1}{4}[\beta_k^2(\lambda_{k2}+2\gamma_{k,22})+(\lambda_{k1}+2\gamma_{k,11})]-\beta_k\gamma_{k,12},\\
P_{k2}&=\tfrac{1}{4}[\alpha_k^2(\lambda_{k2}-2\gamma_{k,22})+(\lambda_{k1}-2\gamma_{k,11})]+\alpha_k\gamma_{k,12}.
\end{aligned} \quad (44)$$

(4) Finally, the Hamiltonian is brought to diagonal form by returning to creation and annihilation operators

$$\begin{aligned}
q_{kt}&=[(P_{kt}/Q_{kt})^{1/2}(1+\alpha_k\beta_k)^{-1}]^{1/2}(c_{kt}+c_{kt}^\dagger),\\
ip_{kt}&=[(Q_{kt}/P_{kt})^{1/2}(1+\alpha_k\beta_k)^{-1}]^{1/2}(c_{kt}-c_{kt}^\dagger),\\
q_{-kt}&=[(Q_{kt}/P_{kt})^{1/2}(1+\alpha_k\beta_k)^{-1}]^{1/2}(c_{-kt}+c_{-kt}^\dagger),\\
ip_{-kt}&=[(P_{kt}/Q_{kt})^{1/2}(1+\alpha_k\beta_k)^{-1}]^{1/2}(c_{-kt}-c_{-kt}^\dagger),
\end{aligned} \quad (45)$$

with

$$[c_{kt},c_{k't'}]=[c_{kt}^\dagger,c_{k't'}^\dagger]=0,$$
$$[c_{kt},c_{k't'}^\dagger]=\delta_{kk'}\delta_{tt'}.$$

Then

$$\mathcal{H}=\mathcal{H}_0+\sum_k C_k+\sum_{k,t=1,2} D_{kt}c_{kt}^\dagger c_{kt}, \quad (46)$$

where the eigenvalues of $c_{kt}^\dagger c_{kt}$ are $n_{kt}=0, 1, 2, \cdots$, and

$$\begin{aligned}
C_k&=R_k+2(1+\alpha_k\beta_k)^{-1}[(Q_{k1}P_{k1})^{1/2}+(Q_{k2}P_{k2})^{1/2}],\\
D_{kt}&=4(1+\alpha_k\beta_k)^{-1}(Q_{kt}P_{kt})^{1/2}.
\end{aligned} \quad (47)$$

The sublattice magnetization is given by

$$M=\frac{kT}{V}\frac{\partial}{\partial H}(\ln Z), \quad (48)$$

where V is the total volume of the system (actually the area for the two-dimensional system under consideration) and Z is the partition function for the sublattice. From (46) the magnetization is found to be

$$M(T,H)=M_s\left\{1-(2NSg\beta)^{-1}\left[\sum_k\frac{\partial C_k}{\partial H}+\sum_{k,t}\frac{\partial D_{kt}}{\partial H}\langle n_{kt}\rangle\right]\right\}, \quad (49)$$
$$\langle n_{kt}\rangle=[\exp(D_{kt}/kT)-1]^{-1}.$$

The evaluation of the partial derivatives is tedious but straightforward and will not be given here.

APPENDIX II

We add to the Hamiltonian of Appendix I the single-ion anisotropy term

$$\mathcal{H}_A=D\sum_{ip}(S_{ip}^y)^2. \quad (50)$$

Transforming to appropriate spin-wave operators gives

$$\mathcal{H}_A=\tfrac{1}{2}DS\sum_{kp}[2a_{kp}^\dagger a_{kp}-a_{kp}a_{-kp}-a_{kp}^\dagger a_{-kp}^\dagger+1]. \quad (51)$$

The terms in (51) also appear in (32) and, hence, the effect of D can be immediately absorbed in the treatment of Appendix I.